Article

Cell

Asymmetric Expression of *LincGET* Biases Cell Fate in Two-Cell Mouse Embryos

Graphical Abstract

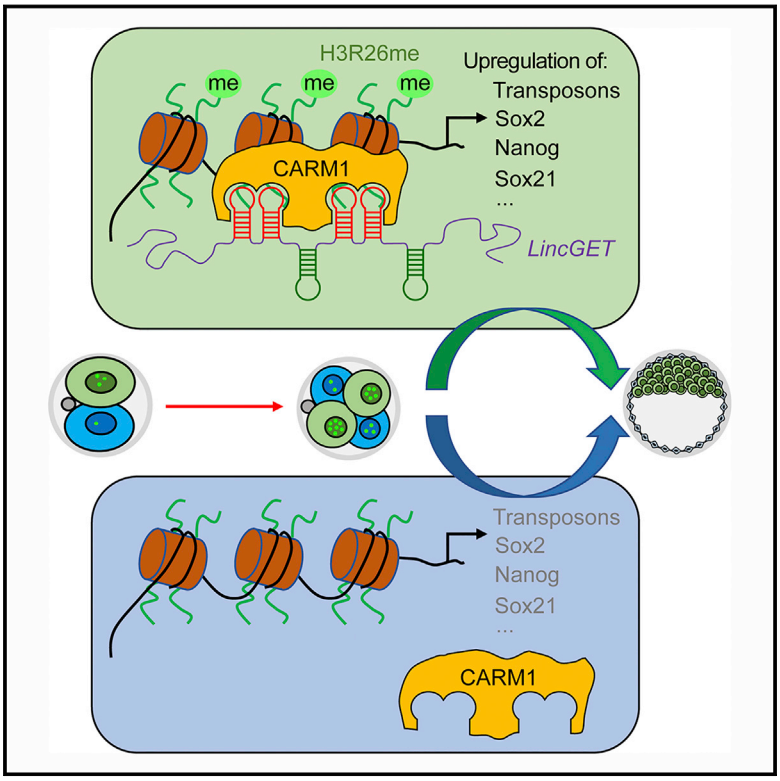

Authors

Jiaqiang Wang, Leyun Wang, Guihai Feng, ..., Zhonghua Liu, Wei Li, Qi Zhou

Correspondence

liwei@ioz.ac.cn (W.L.), qzhou@ioz.ac.cn (Q.Z.)

In Brief

An endogenous retrovirus-associated nuclear long noncoding RNA biases cell fate in mouse two-cell embryos.

Highlights

- *LincGET* is asymmetrically expressed in the nucleus of two- to four-cell mouse embryos
- *LincGET* overexpression biases blastomere fate toward inner cell mass (ICM)
- *LincGET* physically binds to CARM1
- *LincGET*/CARM1 activates ICM-specific genes

Data Resources

GSE110419

Wang et al., 2018, Cell *175*, 1887–1901
December 13, 2018 © 2018 Elsevier Inc.
https://doi.org/10.1016/j.cell.2018.11.039

CellPress

Article

Cell

Asymmetric Expression of *LincGET* Biases Cell Fate in Two-Cell Mouse Embryos

Jiaqiang Wang,[1,2,3,4,8] Leyun Wang,[1,8] Guihai Feng,[1,8] Yukai Wang,[1,8] Yufei Li,[1,2] Xin Li,[5,6] Chao Liu,[1,2] Guanyi Jiao,[1,2] Cheng Huang,[1,2] Junchao Shi,[7] Tong Zhou,[7] Qi Chen,[7] Zhonghua Liu,[4] Wei Li,[1,2,3,*] and Qi Zhou[1,2,3,9,*]

[1]State Key Laboratory of Stem Cell and Reproductive Biology, Institute of Zoology, Chinese Academy of Sciences, 100101 Beijing, China
[2]University of Chinese Academy of Sciences, 100049 Beijing, China
[3]Institute for Stem Cell and Regeneration, Chinese Academy of Sciences, 100101 Beijing, China
[4]College of Life Science, Northeast Agricultural University, 150030 Harbin, China
[5]Institute for Genomic Medicine, University of California, San Diego, CA 92093, USA
[6]Department of Ophthalmology, University of California, San Diego, CA 92093, USA
[7]Department of Physiology and Cell Biology, University of Nevada, Reno School of Medicine, Reno, NV 89557, USA
[8]These authors contributed equally
[9]Lead Contact
*Correspondence: liwei@ioz.ac.cn (W.L.), qzhou@ioz.ac.cn (Q.Z.)
https://doi.org/10.1016/j.cell.2018.11.039

SUMMARY

In early mammalian embryos, it remains unclear how the first cell fate bias is initially triggered and amplified toward cell fate segregation. Here, we report that a long noncoding RNA, *LincGET*, is transiently and asymmetrically expressed in the nucleus of two- to four-cell mouse embryos. Overexpression of *LincGET* in one of the two-cell blastomeres biases its progeny predominantly toward the inner cell mass (ICM) fate. Mechanistically, *LincGET* physically binds to CARM1 and promotes the nuclear localization of CARM1, which can further increase the level of H3 methylation at Arginine 26 (H3R26me), activate ICM-specific gene expression, upregulate transposons, and increase global chromatin accessibility. Simultaneous overexpression of *LincGET* and depletion of *Carm1* no longer biased embryonic fate, indicating that the effect of *LincGET* in directing ICM lineage depends on CARM1. Thus, our data identify *LincGET* as one of the earliest known lineage regulators to bias cell fate in mammalian 2-cell embryos.

INTRODUCTION

Long noncoding RNAs (lncRNAs) have recently emerged as key regulators of many important biological events (Rinn and Chang, 2012), including controlling stem cell pluripotency and differentiation (Guttman et al., 2011; Hu et al., 2012; Ng and Stanton, 2013). However, it remains unknown whether lncRNAs are also actively involved in the process of early embryonic cell fate decision, such as the first lineage segregation that bifurcate the totipotent zygote into the inner cell mass (ICM), which contributes to the fetus, and the trophectoderm (TE), which contributes to the placenta.

In mammalian early embryonic development, the blastomeres within an embryo are morphologically indistinguishable before the eight-cell stage, and their fates are relatively flexible depending on the regulative nature of mammalian embryo development (Rossant and Tam, 2009). However, recent emerging studies have provided compelling evidence that molecular heterogeneity already exists in four- to eight-cell-stage embryos, which predispose the fate of early blastomeres toward either ICM or TE (Goolam et al., 2016; Piotrowska-Nitsche et al., 2005; Plachta et al., 2011; Tabansky et al., 2013; Torres-Padilla et al., 2007; White et al., 2016). To date, the earliest molecular heterogeneity documented was at the four-cell embryo stage. Coactivator-associated arginine methyltransferase 1 (CARM1) was first found asymmetrically distributed between four-cell blastomeres in mice; high CARM1 led to increased levels of histone H3 arginine 26 methylation (H3R26me), which biased the subsequent fate of these blastomeres toward ICM (Torres-Padilla et al., 2007). Recent evidence further showed that high expression of CARM1 at the four-cell stage also increased the OCT4/SOX2-DNA-bound fraction and the expression of its downstream target gene, such as *Sox21* (Goolam et al., 2016; Plachta et al., 2011; White et al., 2016). In addition, PRDM14 was found to be heterogeneously expressed in four-cell-stage embryos, and it interacted with CARM1 to promote H3R26me (Burton et al., 2013). Together, elevation of proteins in the CARM1/PRDM14-OCT4/SOX2-SOX21 axis at the four-cell stage will bias the future progeny of blastomeres toward an ICM fate.

Despite these advances, a key question still remains as to how the observed heterogeneity at the four-cell stage arises in the first place. Is the factor responsible for such heterogeneity buried at the two-cell stage and controlled by upstream regulators? Indeed, with recent research advances using single-blastomere RNA sequencing (RNA-seq), we found that blastomere-to-blastomere heterogeneity already exists at the two-cell stage (Shi et al., 2015). Moreover, we recently found that an endogenous retrovirus (ERV)-associated lncRNA, *LincGET*, was expressed along with zygotic genome activation (ZGA) and specifically persisted through the late two- to four-cell mouse embryo stage, and that *LincGET* was essential for

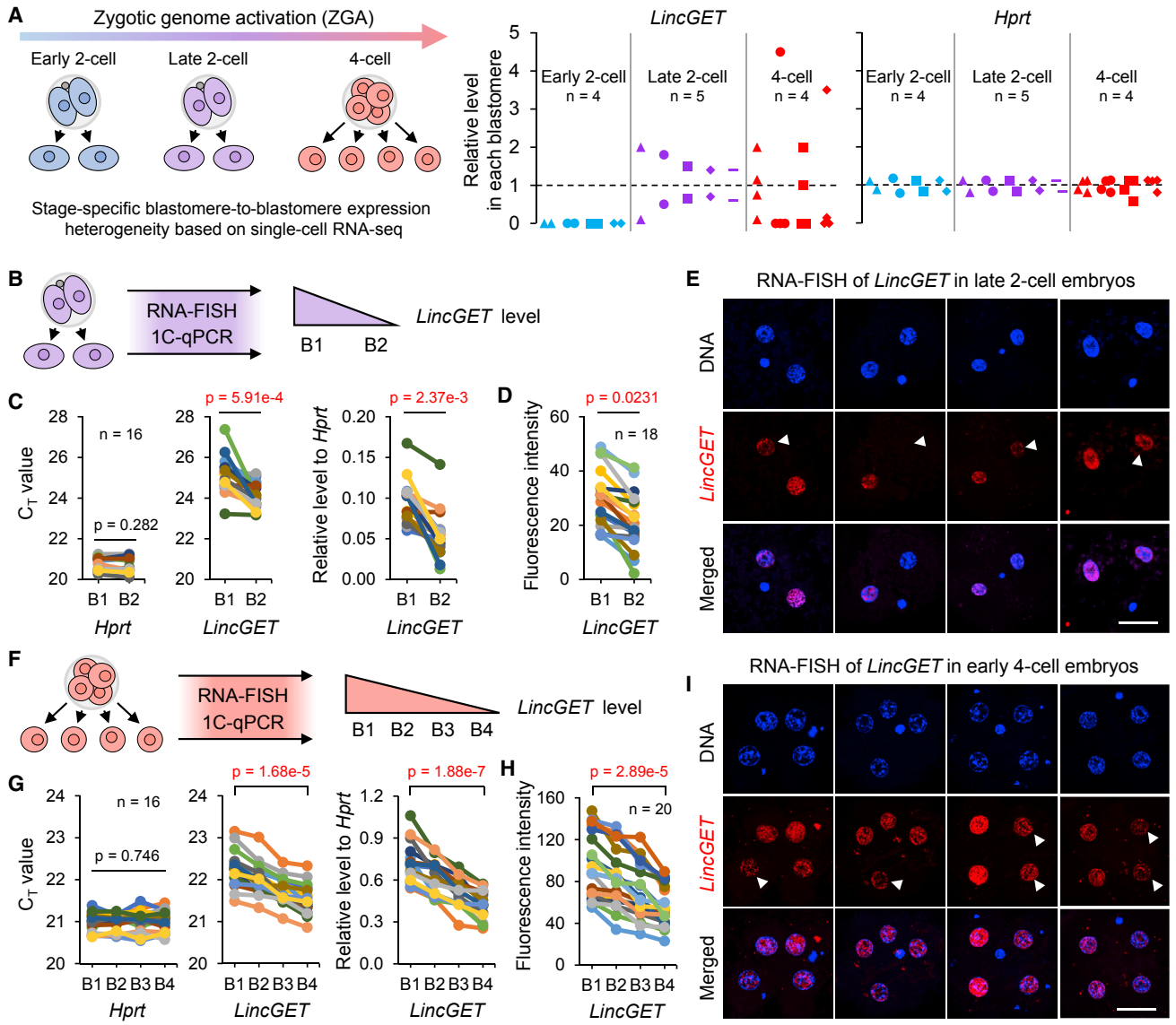

Figure 1. *LincGET* is Transiently Expressed and Asymmetrically Distributed in Two- to Four-Cell Blastomeres

(A) *LincGET* expression is heterogeneous (compared with *Hprt*) in two- to four-cell embryos, according to the bioinformatic analyses of single-blastomere RNA-seq data. Hprt work as a control that is symmetry distributed among blastomeres in two- to four-cell embryos.

(B and F) Schematic overview. Late two-cell (B) or early four-cell (F) embryos were harvested for RNA-FISH and digested into single blastomeres for single-cell (1C)-qPCR. Blastomeres are named B1 and B2 (B) or B1 to B4 (F) according to decreasing *LincGET* concentration.

(C and G) 1C-qPCR results showing *LincGET* distribution asymmetry between blastomeres of late two-cell embryos (C) or among blastomeres of early four-cell embryos (G), but not the housekeeping gene, *Hprt*. CT values are used for level analysis. Two-tailed Student's t tests were used for the statistical analysis.

(D and H) Quantification of RNA-FISH fluorescence intensity of embryos in (B) and (F) showing the asymmetric distribution of *LincGET* at the late two-cell (D) or early four-cell (H) stage. Intensity relative to DNA signal was used.

(E and I) Examples of RNA-FISH of late two-cell (E) or early four-cell (I) embryos. Nuclei with lower *LincGET* are marked by white arrow heads. Three experimental replicates were performed. Scale bar, 50 μm.

See also Figure S1.

embryo development (Wang et al., 2016). Intriguingly, when we analyzed blastomere-to-blastomere heterogeneity of *LincGET* expression using single-blastomere RNA-seq datasets (Deng et al., 2014), we found that its level of expression from the late two-cell blastomere stage became unequal, and this asymmetric distribution was further enhanced in four-cell blastomeres (Figure 1A). These observations led to the present systematic analyses of the heterogeneity of *LincGET* in mouse early embryos and its role in regulating CARM1 level and function to bias the first fate of the embryonic cell.

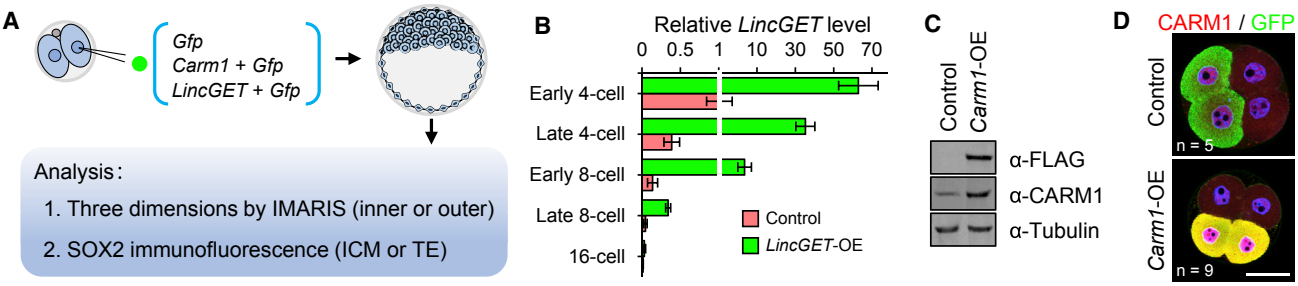

E

Group	Blastocysts 3D (%)	Total cells (n)	Inner cells (%)	GFP cells (%)	Inner cells that are GFP$^+$ (%)	GFP cells that are inner (%)
Gfp	65 (82.65)	41.91 ± 8.79	(37.68 ± 3.43)	(49.02 ± 3.44)	(53.06 ± 8.03) ^{x}	(40.51 ± 4.60) ^{x}
Carm1 + Gfp	63 (84.47)	43.65 ± 10.09	(37.05 ± 2.87)	(48.16 ± 3.02)	(82.45 ± 11.10) ^{y}	(63.38 ± 8.55) ^{y}
LincGET + Gfp	64 (85.18)	47.58 ± 10.35	(37.27 ± 2.52)	(48.40 ± 2.79)	(85.15 ± 9.17) ^{y}	(65.52 ± 7.26) ^{y}

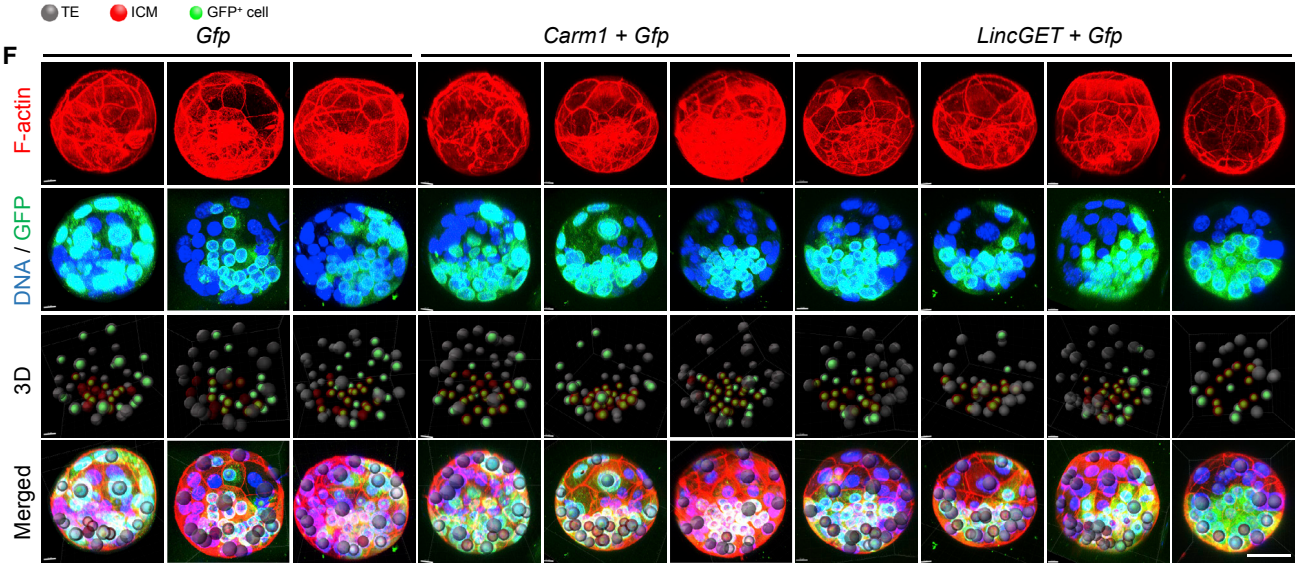

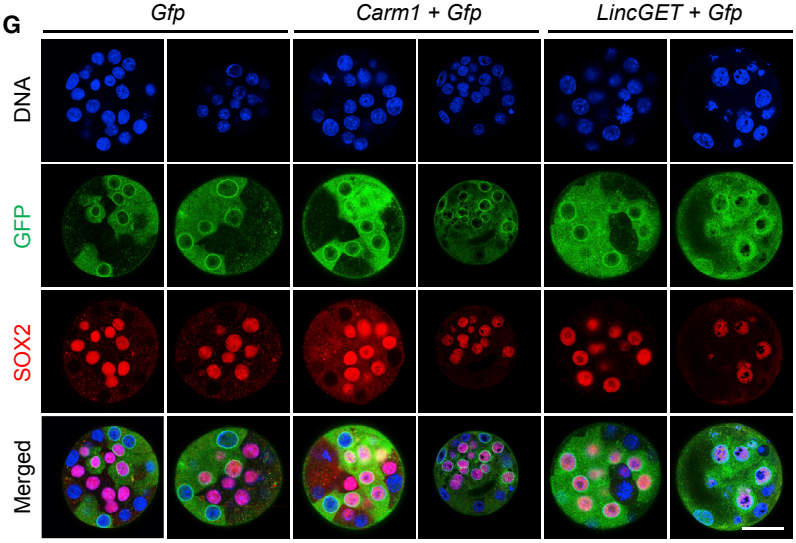

H

Group	Cross sections	GFP cells that are SOX2$^+$ (%)
Gfp	7	(43.57 ± 11.39) ^{x}
Carm1 + Gfp	7	(74.63 ± 15.05) ^{y}
LincGET + Gfp	7	(84.22 ± 14.45) ^{y}

(legend on next page)

RESULTS

LincGET is Transiently Expressed and Asymmetrically Distributed in Two- to Four-Cell Blastomeres

To systematically examine the spatiotemporal expression of *LincGET* in early mouse embryos, we performed fluorescence *in situ* hybridization (FISH) and quantitative PCR with TaqMan probe (TM-qPCR), targeting the *LincGET*-specific region (2,591–2,780 nt) (Figure S1A) throughout mouse early preimplantation embryo development. The TM-qPCR results reinforced our bioinformatics analysis, showing transient *LincGET* expression at the two- to four-cell stage (Figures S1B and S1C). Moreover, the FISH (Figure S1D) and northern blotting (Figure S1E) analyses further confirmed that *LincGET* expression is restricted to the nuclei, appearing first at the early two-cell stage followed by upregulation through the late two-cell to early four-cell stage, downregulation through the late four-cell to early eight-cell stage, and subsequently lack of detection at the late eight-cell stage.

Notably, we observed heterogeneous *LincGET* expression in two- to four-cell embryos based on fluorescence intensity and single-blastomere TM-qPCR (1C-qPCR) analyses, which was consistent with our bioinformatics analyses (Figure 1A). Blastomere-to-blastomere expression of *LincGET* was highly variable between two-cell (Figures 1B–1E) and four-cell blastomeres (Figures 1F–1I) compared to the overall equal expression of *Hprt* between blastomeres (Figures 1C and 1G). Moreover, it is notable that the extent of heterogeneous expression of *LincGET* in four-cell blastomeres was further increased compared to that in two-cell embryos (Figures 1C and 1G). Together, these data raised the possibility that *LincGET* may play a role in directing the developmental fates of early blastomeres.

Increased *LincGET* Biased Blastomeres toward an ICM Fate

To test whether *LincGET* plays a role in biasing early blastomere fate, we overexpressed *LincGET* by injecting *LincGET* RNA into one of the two-cell blastomeres, with a co-injection of green fluorescent protein-Klarsicht/ANC-1/Syne-1 homology (GFP-KASH; *Gfp*) RNA as a lineage tracer, and then monitored embryo development to the blastocyst stage (Figure 2A). We documented an elevated level of *LincGET* by TM-qPCR at the four- to eight-cell stages after two-cell stage overexpression, yet the elevation quickly decreased by the late eight-cell stage and decreased almost down to normal levels at the 16-cell stage (Figure 2B). These findings suggested that the turnover of injected *LincGET* RNA was regulated similarly to the endogenously expressed *LincGET*.

To examine the function of *LincGET* in biasing early embryonic fate, we also performed a parallel *Carm1*-overexpression analysis as a positive control. This was achieved by similarly injecting *Carm1* mRNA and the *Gfp* tracer into one of the two-cell blastomeres followed by expression validation at the four-cell stage (Figures 2C and 2D), as previous research has demonstrated that overexpression of *Carm1* in one of the two-cell blastomeres can bias embryo lineage fate (Torres-Padilla et al., 2007). Injection of only the *Gfp* tracer into one of the two-cell blastomeres served as a negative control. The embryos overexpressing either *LincGET* or *Carm1* (about 150 ng/μL) developed normally and reached the blastocyst stage and birth similar to those injected with only the *Gfp* tracer (Figure 2E and Table S1), showing that overexpression of *LincGET* or *Carm1* does not adversely affect embryo development.

We next analyzed the GFP-positive cell population in the resulting blastocysts from the three experimental groups (*Gfp* only, *LincGET + Gfp*, and *Carm1 + Gfp*). The blastocysts used for cell allocation analysis were processed for cortical F-actin staining to show membrane boundaries (Torres-Padilla et al., 2007) such that the contribution of GFP-labeled cells to the inner (ICM) or outer (TE) layer of the blastocyst could be distinguished and analyzed (Figure 2E). As shown in Figure 2E, the total number of cells in blastocysts and the percentage of GFP-positive cells were similar among different groups. However, the percentage of GFP-positive cells in the ICM was significantly higher in the *LincGET + Gfp* (85.15% ± 9.17%) and *Carm1 + Gfp*

Figure 2. Increased *LincGET* Biased Blastomeres toward an ICM Fate

(A) Schematic overview. RNA (*Gfp*, *Carm1 + Gfp*, or *LincGET + Gfp*) was injected into one blastomere of late two-cell embryos, and the distributions of GFP-positive cells were analyzed at the blastocyst stage (1) in three dimensions to view the inner or outer patterns and (2) by SOX2 immunofluorescence (IF) for the ICM or TE pattern. Nuclear-membrane-localized GFP-KASH (*Gfp*) was used as a lineage tracer.

(B) TM-qPCR results confirming the overexpression of *LincGET*. Three experimental replicates were performed. The error bars represent SEM.

(C and D) Western blot (C) and IF (D) results confirming the overexpression of CARM1. Three experimental replicates were performed. OE, overexpression; α-, anti-. Scale bar, 50 μm.

(E) Analysis of the distribution of progeny of injected blastomere at the blastocyst stage based on 3D reconstruction. Data were represented as mean ± SEM. Two-tailed Student's t tests were used for statistical analysis. Different letters (between x and y) indicate very significant differences ($p < 0.00001$). Key to table headings: blastocyst 3D (%) is the number and developmental rate of blastocysts that were all used for the 3D analysis, total cells (n) is the total number of cells in the blastocyst, inner cells (%) is the percentage of inner cells out of the total number of cells in the blastocyst, GFP cells (%) is the percentage of GFP-positive cells out of the total number of cells in the blastocyst, GFP cells that are inner (%) is the percentage of GFP-positive inner cells out of the total number of GFP-positive cells in the blastocyst, inner cells that are GFP^+ (%) is the percentage of GFP-positive inner cells out of the total number of inner cells in the blastocyst, and GFP cells that are inner (%) is the percentage of GFP-positive inner cells out of the total number of total cells in the blastocyst.

(F) Examples of 3D analysis results. Scale bar, 50 μm.

(G) SOX2 and GFP fluorescent staining of blastocysts. SOX2 was used as an ICM marker. The results show that most SOX2-positive cells are GFP-positive in embryos injected with *Carm1* and *Gfp* (*Carm1 + Gfp* lane) or *LincGET* and *Gfp* (*LincGET + Gfp* lane), but not in embryos injected with only *Gfp* (*Gfp* lane). Three experimental replicates were performed. Scale bar, 50 μm.

(H) Statistical data of the percentages of GFP- and SOX2-positive cells out of the SOX2-positive cells of embryos in (G) and Figure S2C. About 40% of GFP-positive cells were SOX2-positive in the control group, while the percentage was about 80% for the *Carm1 + Gfp* and *LincGET + GFP* groups. Two-tailed Student's t tests were used for statistical analysis. Different letters (between x and y) indicate very significant differences ($p < 0.00001$).

See also Figure S2, and Tables S1, S2, and S3.

A

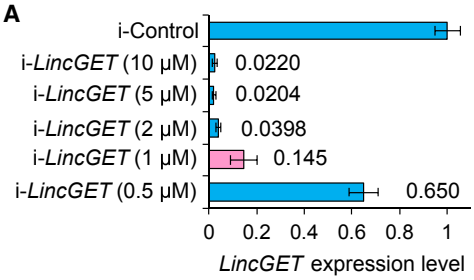

B

Group	Concentration	Injected 2C	4C(%)	BL(%)
i-Control	10 μM	41	39 (90.70)	36 (83.72)
i-*LincGET* 10 μM	10 μM	77	0 (0.00)	0 (0.00)
i-*LincGET* 5 μM	5 μM	84	1 (1.19)	0 (0.00)
i-*LincGET* 2 μM	2 μM	76	1 (1.32)	0 (0.00)
i-*LincGET* 1 μM	1 μM	74	55 (73.33)	33 (44.22)
i-*LincGET* 0.5 μM	0.5 μM	75	70 (94.59)	66 (89.19)

C

Group	Blastocysts 3D (%)	Total cells (n)	Inner cells (%)	GFP cells (%)	Inner cells that are GFP$^+$ (%)	GFP cells that are inner (%)
Gfp	65 (82.65)	41.91 ± 8.79	(37.68 ± 3.43)	(49.02 ± 3.44) ^{x}	(53.06 ± 8.03) ^{x}	(40.51 ± 4.60) ^{x}
i-Control + *Gfp*	36 (83.72)	39.17 ± 6.58	(37.44 ± 3.10)	(49.31 ± 2.84) ^{x}	(54.76 ± 8.00) ^{x}	(41.41 ± 5.47) ^{x}
i-*LincGET* + *Gfp*	33 (44.22)	37.82 ± 6.59	(34.97 ± 2.56)	(40.11 ± 5.17) ^{y}	(31.74 ± 10.49) ^{y}	(27.65 ± 8.41) ^{y}

D

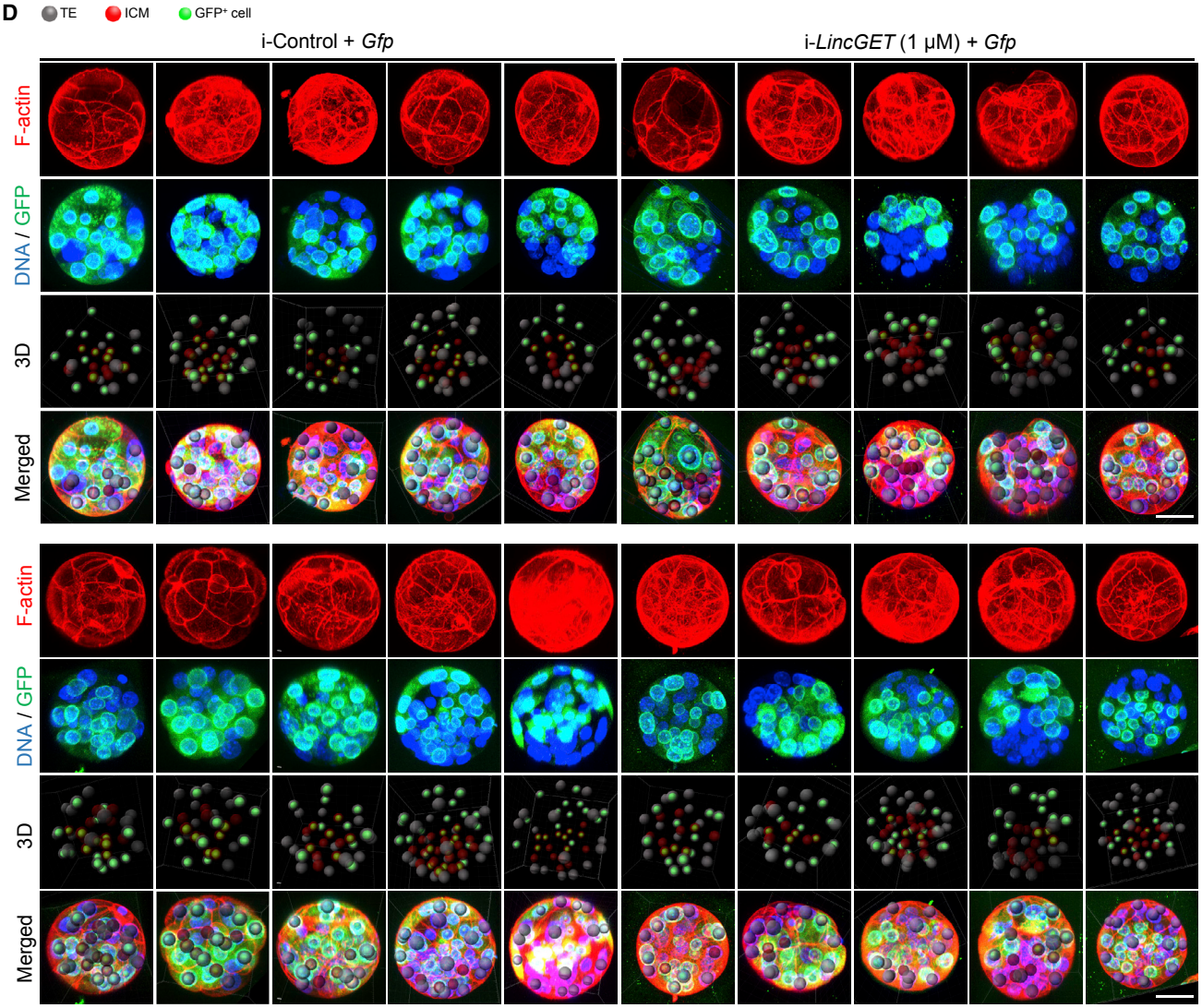

(legend on next page)

(82.45% ± 11.10%) groups than in the *Gfp* only (53.06% ± 8.03%) group (Figures 2E, 2F, S2A, and S2B, and Table S2). Moreover, we examined the expression of SOX2 as an ICM marker in the blastocysts from the three groups and found that the percentage of SOX2-positive cells at the blastocyst stage was much higher in GFP-positive cells derived from both the *LincGET + Gfp* (84.22% ± 14.45%) and *Carm1 + Gfp* (74.63% ± 15.05%) groups than the *Gfp* only (43.57% ± 11.39%) group (Figures 2H and S2C and Table S3). These results demonstrated that forced overexpression of *LincGET* in one of the two-cell blastomeres biased its progeny cells toward an ICM fate.

In order to exclude the possibility that the phenotypic observations may be caused by the large amounts of synthetic RNA being injected, we injected a set of controls: *Dyei*, another mouse ERV-associated lncRNA that has been identified from the genome locus near *LincGET* (between Dyrk1b and Eid2 on chromosome 7) and expressed at the two- to four-cell stages (Wang et al., 2016); *pancIl17d*, a promoter-associated nocoding RNA with interleukin-17d, which is expressed at the two- to four-cell stages and promotes the expression of interleukin-17d from the four-cell stage (Hamazaki et al., 2015); 1–2,570 nt of *LincGET*; 3,940–6,285 nt of *LincGET*; and antisense of ampicillin restriction gene (*antiAmpR*). We found that all of these controls have no effect on preimplantation development, as blastocyst rate and GFP-positive cell rate were normal, and none of the controls could bias fate (Figure S3).

Knockdown of *LincGET* Expression Prevents Blastomeres from Undergoing an ICM Fate

On the other hand, we wondered whether *LincGET* knockdown could prevent blastomeres from undergoing an ICM fate. Our previous study showed that near-complete depletion of *LincGET* in single-cell embryos resulted in a two-cell-stage arrest (Wang et al., 2016), suggesting *LincGET* played an essential role in early embryo development. Thus, to study how *LincGET* knockdown affected cell fate, we performed a knockdown titration assay. The knockdown reagent locked nucleic acid (LNA) was injected into single blastomeres of two-cell embryos at different concentrations followed by analysis of the effect on embryo development. *LincGET* LNA injection into single blastomeres of two-cell embryos at 10 μM, 5 μM, or 2 μM resulted in more than 94% deletion of *LincGET*, and nearly all injected blastomeres exhibited two-cell-stage developmental arrest (Figures 3A and 3B). Besides, *LincGET* LNA injection at 1 μM depleted about 85.5% of total *LincGET*, and 44% of injected blastomeres could still develop to the blastocyst stage while others arrested at the two-cell stage (Figures 3A and 3B). Moreover, injection of *LincGET* LNA at 0.5 μM was unable to knock down *LincGET* efficiently and had little effect on preimplantation development of injected blastomeres (Figures 3A and 3B).

We therefore analyzed the fate choice in the blastocysts after injection of 1 μM *LincGET* LNA into single blastomeres at the two-cell stage. The ratio of progeny with an ICM fate was significantly reduced when the blastomeres were injected with the *LincGET* LNA compared with blastomeres without injection or injected with the control LNA, indicating that a lower level of *LincGET* prevented blastomeres undergoing an ICM fate (Figures 3C and 3D). Furthermore, we found that these blastocysts had a lower percentage of GFP-positive cells (Figures 3C and 3D), indicating that lower levels of *LincGET* do harm preimplantation development.

LincGET and CARM1 Form a Complex

By performing co-localization of *LincGET* via FISH and CARM1 via immunofluorescence staining (IF combined with FISH [IF-coFISH]), we found that in most of the examined early four-cell embryos (eight out of nine), the nuclear intensity of *LincGET* and CARM1 were positively correlated (Figures 4A, 4B, and S4). Moreover, we found that the signals of *LincGET* and CARM1 largely overlapped in the nuclei of early four-cell blastomeres, and more CARM1 located to the nucleus where *LincGET* is higher (Figures 4A and S4). These data raised the possibility that *LincGET* may physically interact with CARM1 to form a functional complex and promote CARM1 nuclear location. We also injected *Dyei* into single-cell embryos (1–2 pL, 150 ng/μL, because its level is very low in four-cell embryos) and performed IF-coFISH at the four-cell stage as a staining control. The results show that *Dyei* does not co-localize with CARM1 (Figure S5).

We separated four-cell embryos into cytoplasmic and nuclear fractions, one blastomere of which was injected with *LincGET* + *Gfp*, *Gfp* only, or *Dyei* + *Gfp* at two-cell stage, and evaluated CARM1 protein level by western blotting. The results showed that *LincGET*, but not *Dyei* or *Gfp* overexpression increased the nuclear percentage of CARM1 (Figure 4C). We

Figure 3. Knockdown of *LincGET* Expression Prevents Blastomeres from Undergoing an ICM Fate

(A) Titration study to knock down *LincGET* using LNA at different concentrations. The TM-qPCR results showed that LNA injection at 10 μM, 5 μM, or 2 μM resulted in more than 94% deletion of *LincGET*; LNA injection at 1 μM and 0.5 μM resulted in depletion of 85.5% and 35% of total *LincGET* level, respectively. Three experimental replicates were performed. The error bars represent SEM.

(B) Preimplantation developmental rate upon *LincGET* knockdown by LNA injection in one blastomere at the two-cell stage. Nearly all the injected blastomeres were arrested at the two-cell stage when injected with *LincGET* LNA at 10 μM, 5 μM, or 2 μM; 44% of blastomeres injected with *LincGET* LNA at 1 μM could develop to blastocyst stage; and *LincGET* LNA injection at 0.5 μM had no effect on preimplantation development of injected blastomeres.

(C) Analysis of the distribution of progeny of injected blastomeres at the blastocyst stage based on 3D reconstruction. LNA for *LincGET* was at 1 μM. Data are shown as mean ± SEM. Two-tailed Student's t tests were used for statistical analysis. Different letters (between x and y) indicate very significant differences ($p < 0.00001$). Key to table headings: blastocyst 3D (%) is the number and developmental rate of blastocysts that were all used for 3D analysis, total cells is the total number of cells in the blastocyst, inner cells (%) is the percentage of inner cells out of the total number of cells in the blastocyst, GFP cells (%) is the percentage of GFP-positive cells out of the total number of cells in the blastocyst, GFP cells that are inner (%) is the percentage of GFP-positive inner cells out of the total number of GFP-positive cells in the blastocyst, and inner cells that are GFP^+ (%) is the percentage of GFP-positive inner cells out of the total number of inner cells in the blastocyst.

(D) Examples of 3D analysis results. Scale bar, 50 μm.

See also Table S2.

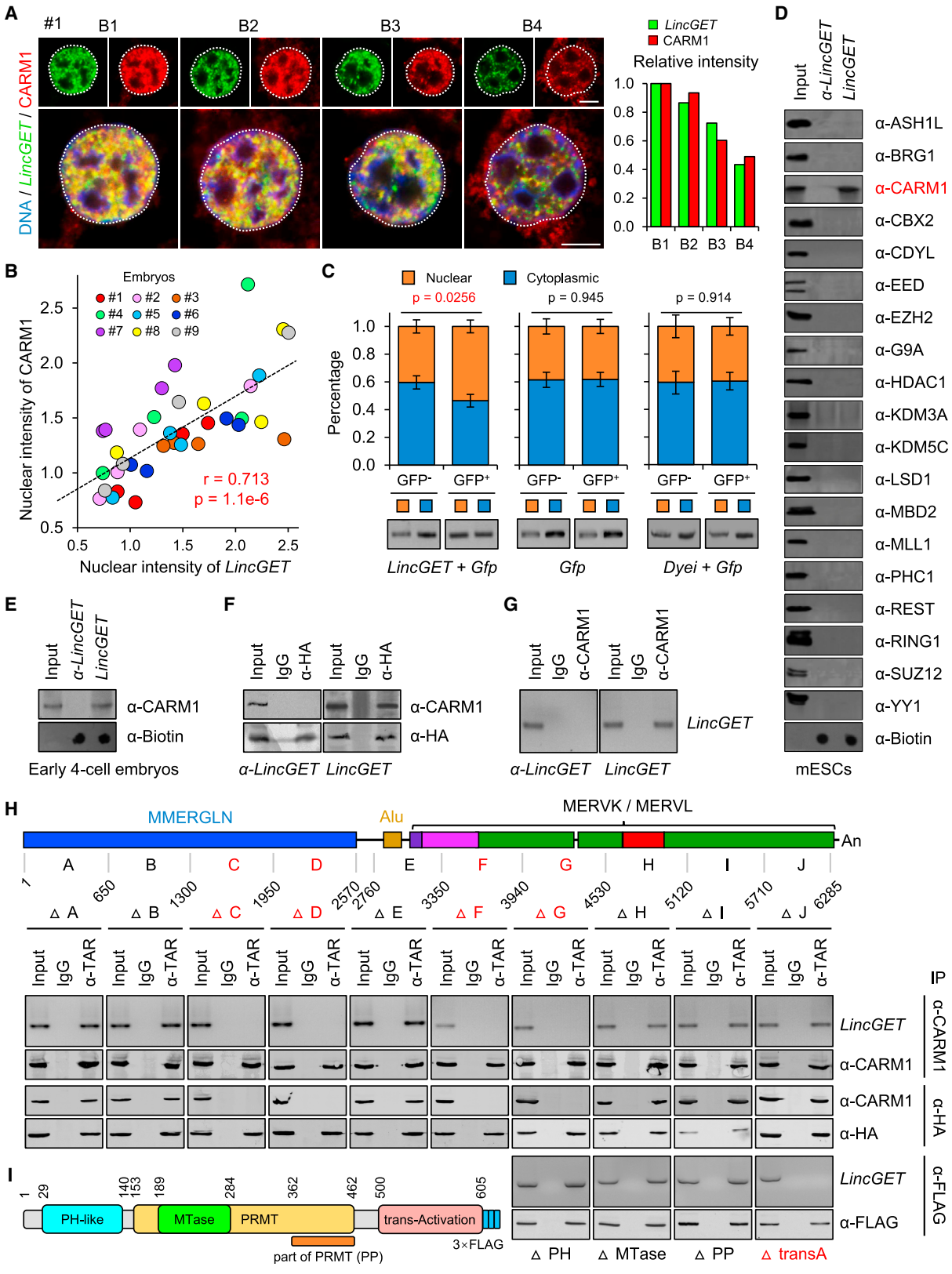

(legend on next page)

next performed RNA pull-down followed by western blotting with biotin-labeled *LincGET* using lysates from mESCs or early four-cell embryos (~2,600 embryos were collected for preparing the lysates for each group). The results showed that *LincGET* prefer to form a complex with CARM1 rather than other well-known epigenetic modifiers such as BRG1, EZH2, G9A, HDAC1, LSD1, SUZ12, and YY1 (Figures 4D and 4E). Moreover, we performed RNA pull-down followed by mass spectrometry using lysates from mESCs and identified 64 *LincGET*-specific binding proteins (*anti-LincGET* as control), which contain CARM1 but no other well-known epigenetic modifiers (Table S4).

Further, we constructed a fused *LincGET-MS2* RNA, whereby a minimal hairpin aptamer (named MS2) was linked to the 5′ end of *LincGET*. The MS2 region of the fused *LincGET-MS2* RNA could selectively bind to dimerized MS2 bacteriophage coat proteins (MS2P) (Peabody, 1993) and thus could be used for coimmunoprecipitation (coIP) experiments. The coIP experiments using mESCs expressing *LincGET-MS2*-fused RNAs and HA-tagged MS2P showed that *LincGET* indeed forms an RNA-protein complex with CARM1 (Figure 4F). Moreover, RNA IP (RIP) of *LincGET* in mESCs transiently overexpressing *LincGET* further confirmed the *LincGET*-CARM1 complex (Figure 4G).

To further identify the functional domain of *LincGET* that interacts with CARM1, we generated a series of truncated *LincGET* RNAs marked with MS2 (Figure 4H) followed by coIP and RIP assays with CARM1. Our data demonstrated that fragments of nucleotides 1,301–2,570 and 3,351–4,530 of *LincGET* were essential for binding to CARM1 (Figure 4H).

We next examined the protein site in CARM1 that interacts with *LincGET*. We constructed four 3 × FLAG-tagged truncated CARM1 mutants with deletion of the pleckstrin homology (PH)-like domain (Δ PH), methyltransferase (MTase) domain (Δ MTase), part of the protein arginine methyltransferase (PRMT) domain (Δ PP), or *trans*-activation domain (Δ transA), respectively. We then performed the RIP assays using mouse epiblast stem cells (mEpiSCs) overexpressing full-length *LincGET* and each of the truncated CARM1 mutants. The results show that the transA domain of CARM1 is essential for *LincGET* binding (Figure 4I).

LincGET/CARM1 Complex Promoted H3R26me2 and Activated ICM Gene Expression

We further examined whether expression of *LincGET* in an early embryo could promote the known events downstream of CARM1, such as the establishment of H3R26me (Torres-Padilla et al., 2007) and expression of genes that promote/represent an ICM fate, such as *Sox2* (Torres-Padilla et al., 2007), *Nanog* (Torres-Padilla et al., 2007), and *Sox21* (Goolam et al., 2016) (Figure 5A). Our results showed that overexpression of *Carm1* or *LincGET* similarly enhanced H3R26me2 levels at the eight-cell stage (Figure 5B) and increased *Nanog*, *Sox2*, and *Sox21* at both RNA and protein levels (Figures 5C–5F). In addition, we found that CDX2 expression at the eight-cell stage was inhibited upon *Carm1* or *LincGET* overexpression (Figure 5G). Notably, the expression level of *Oct4* was not significantly influenced by overexpression of *Carm1* or *LincGET* (Figure S6A). The overall elevated levels of ICM-specific genes in the progeny of *LincGET-*/*Carm1*-overexpressing blastomeres is consistent with and could explain the effect of the *LincGET*/*Carm1* complex in biasing blastomere fate toward ICM.

Given the complex feedback/feedforward nature of ICM fate/pluripotency network, we wonder whether those ICM-specific pluripotent factors overexpression, such as *Nanog*, might also induce *LincGET* expression. As a result, we found *Carm1* overexpression, but not *Nanog* overexpression, would induce *LincGET* expression (Figure S6B).

LincGET/CARM1 Complex Increased Global Chromatin Accessibility

We next explored the potential mechanisms by which the *LincGET*/CARM1 complex activates ICM-specific genes at the

Figure 4. *LincGET* and CARM1 Form a Complex

(A) IF combined with FISH results show *LincGET* and CARM1 co-localization in the nucleus of early four-cell embryos. The intensity analysis of this embryo stage shows that *LincGET* and CARM1 are linearly correlated and different among four blastomeres. The relative intensity of *LincGET*/CARM1 (green/red) to nucleus DNA (blue) was used for comparison, which could reduce errors caused by the depth of the nucleus between blastomeres. Scale bar, 10 μm.

(B) The intensity (relative to DNA signals) analysis of nine embryos shows that *LincGET* and CARM1 are linearly correlated and different among four blastomeres of a four-cell embryo. The correlation coefficient (r) and p value are determined by Pearson's correlation.

(C) CARM1 fractionation analysis showed *LincGET* overexpression, but not *Dyei* or *Gfp* overexpression, increased the percentage of nuclear CARM1. The four-cell embryos, one blastomere of which was injected with *LincGET*/*Gfp* or *Gfp* only at the two-cell stage, were separated into cytoplasmic and nuclear fractions. The CARM1 protein level of each fraction was evaluated by western blotting. More than 400 four-cell embryos were used for each replicate, and three experimental replicates were performed. Isoform abundance on SDS-PAGE gels was measured in ImageJ. Three experimental replicates were performed. The error bars represent SEM. Two-tailed Student's t tests were used for statistical analysis.

(D) RNA pull-down-western blotting using biotinylated *LincGET* or *antisense-LincGET* (*α-LincGET*) with mESCs lysates (left) shows that *LincGET* interacts with CARM1. Three experimental replicates were performed. Two-tailed Student's t tests were used for statistical analysis. α-, anti-.

(E) RNA pull-down western blotting using biotinylated *LincGET* or *antisense-LincGET* (*α-LincGET*) with early four-cell-stage embryo (about 2,600 embryos were used for each experiment) lysates. Three experimental replicates were performed. α-, anti-.

(F) CoIP results using mEpiSCs expressing HA-MS2P with MS2-labeled *LincGET* or *antisense-LincGET* (*α-LincGET*) and anti-HA antibody. The results show that *LincGET* forms an RNA-protein complex with CARM1. Three experimental replicates were performed. α-, anti-.

(G) RIP assays with *LincGET*-expressing mEpiSCs showing that *LincGET* can bind to CARM1. Three experimental replicates were performed. α-, anti-.

(H) CoIP followed by RT-PCR or western blot using mEpiSCs expressing HA-MS2P with MS2-labeled *LincGET* mutants. The results show that the *LincGET* mutants with 1,301–1,950-nt, 1,951–2,570-nt, 3,351–3,940-nt, or 3,941–4,530-nt deletions could not bind CARM1, while other mutants could. Three experimental replicates were performed.

(I) RIP assays with *LincGET*-expressing mEpiSCs expressing *LincGET* and one of the various CARM1 mutants show that the transA domain of CARM1 is essential for binding with *LincGET*. Three experimental replicates were performed. α-, anti-.

See also Figures S4 and S5.

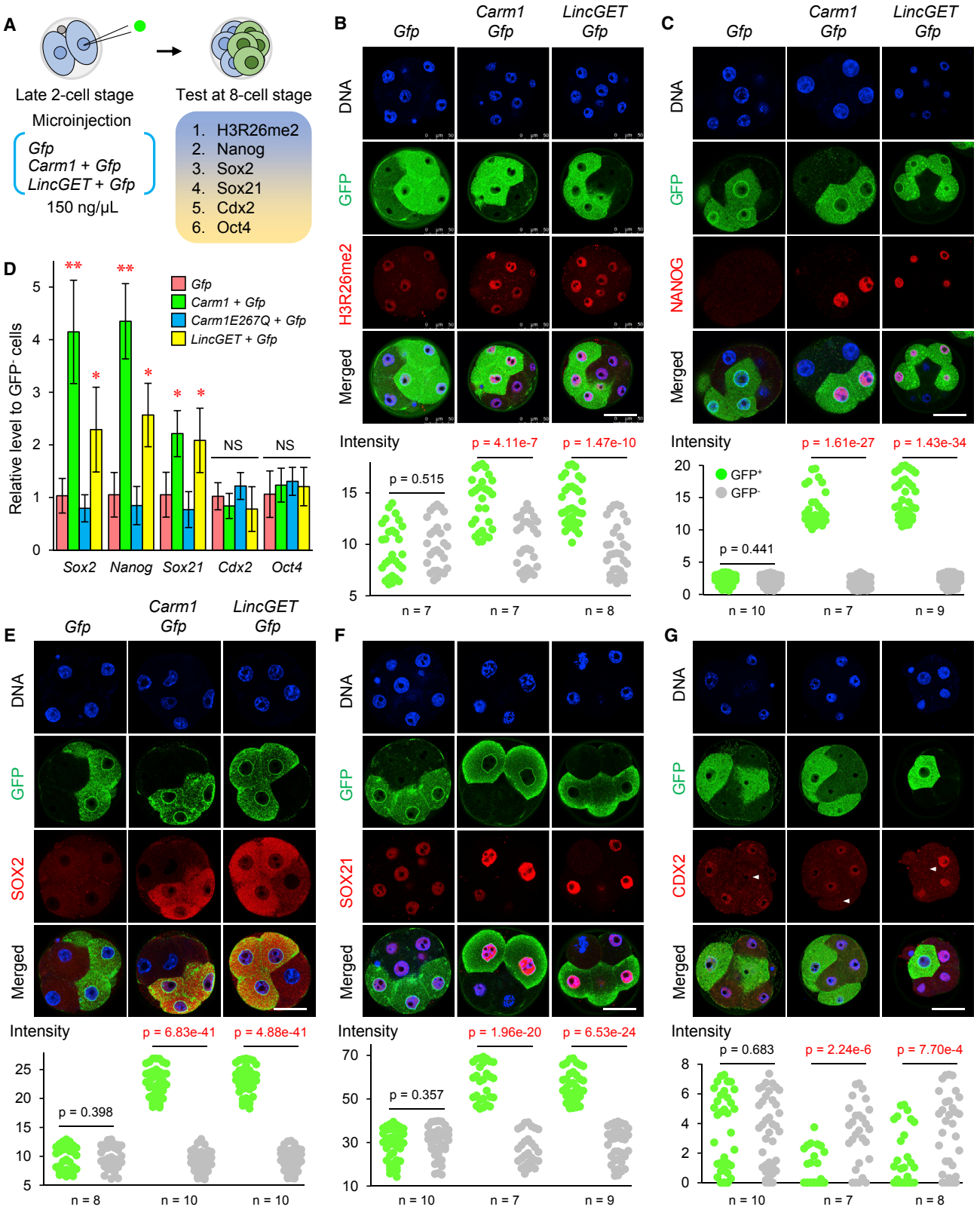

(legend on next page)

eight-cell stage and hypothesized that this may result from altered chromatin accessibility at the promoter regions of these genes. To test this hypothesis, we examined chromatin accessibility by preforming an assay for transposase-accessible chromatin with high-throughput sequencing (ATAC-seq) (Wu et al., 2016). The results showed that the promoters of ICM-specific genes (1,168 genes) (Liu et al., 2016) were more open in *LincGET*- or *Carm1*-overexpressing blastomeres at the eight-cell stage. On the contrary, the chromatin of TE-specific gene (757 genes) (Liu et al., 2016) promoter regions was less open compared to in control blastomeres (Figure 6A).

There is a progressive decrease in chromatin openness along with preimplantation development, which is thought to be important for the transition from totipotency to pluripotency (Bošković et al., 2014). Therefore, we speculated the function of *LincGET*/CARM1 complex in biasing ICM fate might be associated with increasing global chromatin accessibility. To examine chromatin accessibility at the single-cell level, we resorted to an imaging-based *in situ* DNase I-terminal deoxynucleotidyl transferase deoxyuridine triphosphate (dUTP) nick-end labeling (TUNEL) assay (Jachowicz et al., 2017), where the fluorescence intensity observed in TUNEL represents a direct measurement of DNase I sensitivity, and thus chromatin accessibility (Figure 6B). As a result, *LincGET* or CARM1 overexpression similarly led to significantly higher levels of TUNEL fluorescence in the daughter cells of the overexpressed rather than the control blastomeres (Figure 6C). Notably, we did not detect differences in levels of phosphorylated histone H2A.X between the daughter cells of the overexpressed and control blastomeres (Figure 6C), suggesting that the observed increase in DNase I sensitivity was not a result of DNA damage. We also compared nuclear volume, another parameter for chromatin openness (Jachowicz et al., 2017), and observed a significant increase in nuclear volume after *LincGET*/CARM1 overexpression compared to control blastomeres (Figure 6C).

We have reported that *LincGET* prefers to activate genes locating close to long terminal repeats (LTRs) in GLN, MERVL, and ERVK (GLKLTRs) (Wang et al., 2016), and it has been reported that transcriptional activation of transposons such as LINE-1 in early embryos could increase global chromatin accessibility and embryonic pluripotency (Jachowicz et al., 2017). It therefore raised a possibility that *LincGET*/CARM1-mediating ICM-specific genes activation may be linked with transposons activation and global chromatin plasticity. To this end, we indeed found that genomic LINE and LTR sequences are in closer distance to ICM- rather than TE-specific genes (Figure 6D). Besides, the qPCR results indeed showed that overexpression of *LincGET* or *Carm1* in one of the two-cell blastomeres increased the expression level of transposons, including GLN, ERVL, ERVK, and LINE-1 in progeny cells at the eight-cell stage (Figure 6E).

Together, these converging pieces of evidence strongly suggest that *LincGET* and CARM1 bias the blastomeres toward an ICM fate by increasing chromatin openness and activating ICM-specific genes. How the chromatin openness induced by *LincGET*/CARM1 favors gene promoters related to ICM rather than TE remains unclear, but it seems that the *LincGET*/CARM1 complex activates transposons and spreads the active chromatin status toward ICM-specific genes, which prefer to locate near transposons.

Interdependence of *LincGET* and CARM1 in Directing ICM fate

Because *LincGET* could potentially interact with multiple proteins in addition to CARM1, we next examined whether CARM1 was the necessary protein partner that enabled *LincGET* to exert its function regarding the biasing of embryonic fate. By simultaneous overexpression of *LincGET* and depletion of *Carm1* using LNA (Figures S7A and S7B) in one of the two-cell blastomeres, we found that once *Carm1* was knocked down, even if the level of *LincGET* was elevated, the progeny blastomeres were no longer biased toward ICM but rather tended to generate TE (Figures 7A, 7B, S7C, and S7D). Correspondingly, depleting *Carm1* in the *LincGET*-overexpressing blastomeres no longer upregulated the expression of *Sox2*, *Nanog*, and *Sox21*, and, in fact, the H3R26me2 level was decreased (Figures 7C, S7E, and S7F). Also, depleting *Carm1* in the *LincGET*-overexpressing blastomeres was associated with decreased DNase I sensitivity and nuclear volume (Figures 7D, S7G, and S7H), suggesting that the chromatin state became more condensed. These data demonstrated that the function of *LincGET* in biasing embryonic fate requires the presence of CARM1.

To further test whether *LincGET* must interact with CARM1 as a complex to exert its function, we next injected truncated *LincGET* without CARM1-binding sites (nucleotides 1,301–2,570 [ΔC–D] or 3,351–4,530 [ΔF–G]) into one of the two-cell blastomeres with or without knocking down *Carm1*. Compared to the injection of intact *LincGET*, the truncated *LincGET* failed to upregulate *Sox2* and *Sox21* in the progeny blastomeres even in the presence of CARM1 (Figure 7E, red). Besides, the intact *LincGET* could not

Figure 5. *LincGET*/CARM1 Complex Promoted H3R26me and Activated ICM Gene Expression

(A) Schematic overview. RNA (*Gfp*, *Carm1* + *Gfp*, or *LincGET* + *Gfp*) was injected into one blastomere of late two-cell embryos, and the levesl of H3R26me2, *Nanog*, *Sox2*, *Sox21*, *Cdx2*, and *Oct4* were tested at eight-cell stage.

(B) H3R26me2 staining of eight-cell embryos shows that *Carm1* or *LincGET* overexpression led to a dramatic increase in H3R26me2 modification. For fluorescence analysis, the green ball stands for GFP^+ cells, and the gray ball stands for GFP^- cells. Three experimental replicates were performed. Scale bar, 50 μm. Two-tailed Student's t tests were used for statistical analysis.

(C–F) NANOG (C), SOX2 (E), and SOX21 (F) were increased in the progeny of *Carm1*- or *LincGET*-injected blastomeres at both the RNA (D) and protein levels. The group names in (F) are the same as in (B); the group names in (G) are the same as in (C). Three experimental replicates were performed. Scale bar, 50 μm. The error bars represent SEM. For fluorescence analysis, the green ball stands for GFP^+ cells and the gray ball stands for GFP^- cells. Two-tailed Student's t tests were used for statistical analysis. Compared to the *Gfp* group, $^{**}p < 0.001$, $^{*}0.01 < p < 0.05$ (not significant [NS]), $p > 0.05$.

(G) No change in CDX2 was found in the progeny of *Carm1*- or *LincGET*-injected blastomeres. Interestingly, CDX2 was detected in only some blastomeres (blastomeres showing no CDX2 expression are marked with white arrowheads). Three experimental replicates were performed. Scale bar, 50 μm. For fluorescence analysis, the green ball stands for GFP^+ cells, and the gray ball stands for GFP^- cells. Two-tailed Student's t tests were used for statistical analysis. See also Figure S6.

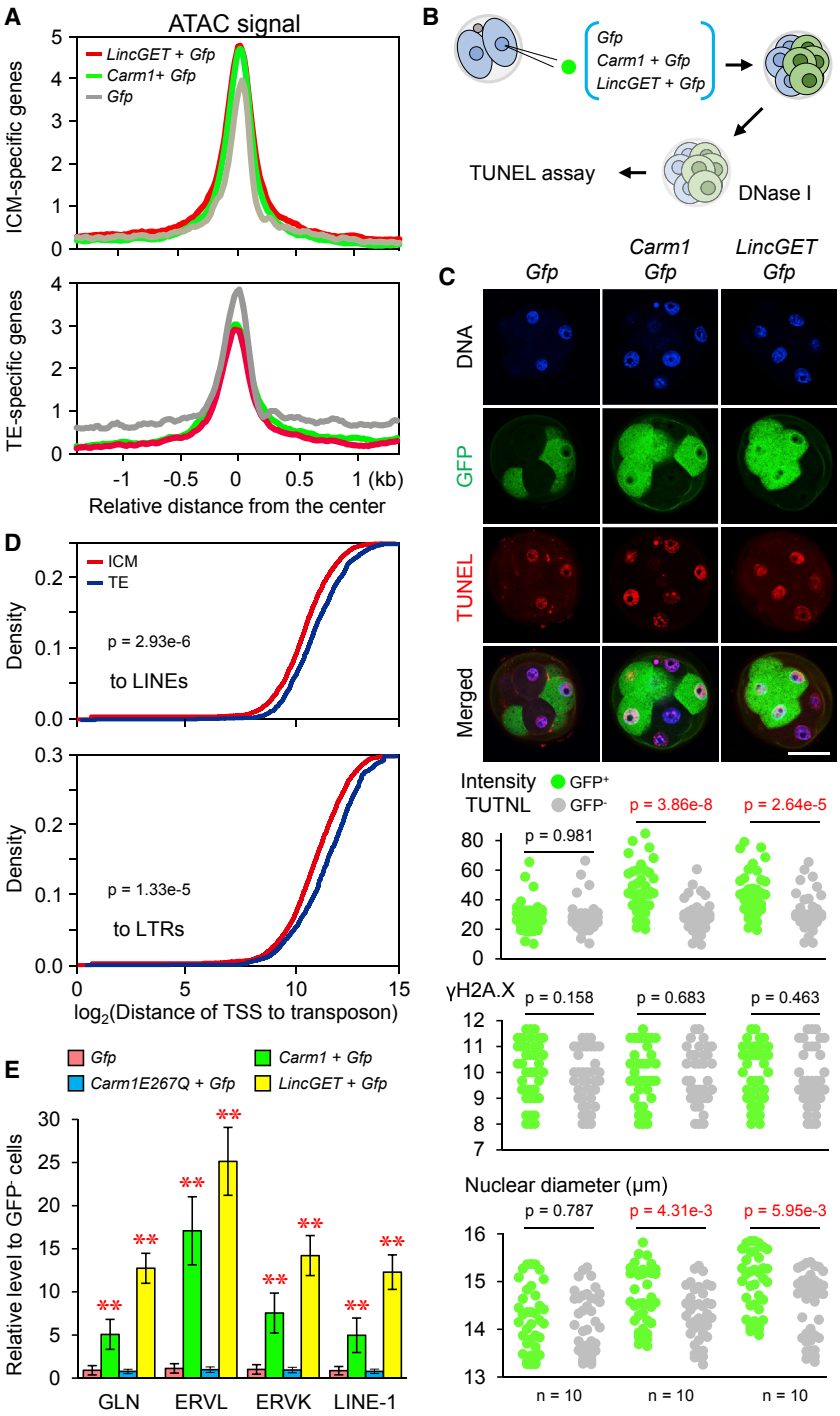

Figure 6. *LincGET*/CARM1 Increased Global Chromatin Accessibility

(A) ATAC-seq results show that the promoters of ICM-specific genes are more open in *LincGET*- or *Carm1*-overexpressing blastomeres, while the chromatin of TE-specific promoter regions is less open compared to in the control blastomeres.

(B) Overview of DNase I-TUNEL assay.

(C) *LincGET* or CARM1 overexpression led to significantly higher levels of TUNEL fluorescence and increased nuclear volume in daughter cells of injected blastomeres. Scale bar, 50 μm. Three experimental replicates were performed. For fluorescence analysis, the green ball stands for GFP^+ cells, and the gray ball stands for GFP^- cells. Two-tailed Student's t tests were used for statistical analysis.

(D) Bioinformatic analysis revealed that genomic LINE or LTR sequences are in closer distance to ICM-specific genes rather than TE-specific genes. Two-sample Kolmogorov-Smirnov tests were used for statistical analysis.

(E) qPCR shows that overexpression of *LincGET* or *Carm1* increased the expression level of transposons such as GLN, ERVL, ERVK, and LINE-1. Three experimental replicates were performed. The error bars represent SEM. Two-tailed Student's t tests were used for statistical analysis. $^{**}p < 0.01$.

upregulate either *Sox2* or *Sox21* when *Carm1* was depleted (Figures 7E and 7F, orange). These results indicated the functional necessity of the *LincGET*-CARM1 complex.

In addition, we found that depletion of *LincGET* led to late two-cell-stage arrest (10 μM LNA with nearly 100% interference efficiency), which could not be rescued by *Carm1* overexpression (Figure S7I), suggesting that *LincGET* is a master regulator upstream of Carm1 and that it may have other essential functions beyond interaction with *CARM1*.

Functional Domain of *LincGET* beyond CARM1 Binding

During our functional screening of truncated *LincGET* mutants, overexpression of several truncated *LincGET* mutants (Δ 2,761–3,350 [ΔE] or Δ 5,121–5,710 [ΔI]) in early-stage embryos led to binding to CARM1 but failed to upregulate *Sox2* and *Sox21* (Figure 7F, green). This suggested that these truncated regions harbor important functional domains. By overexpressing both CARM1 and these *LincGET* mutants, we found that the truncated *LincGET* mutants exerted a dominant-negative effect in cancelling CARM1's function regarding upregulating *Sox2* and *Sox21* (Figure 7G, green). We propose that these functional domains of *LincGET* might be acting as "anchors" to guide the *LincGET*-CARM1 complex to its correct location in the nucleus, without which CARM1 could not function normally event if the *LincGET*-CARM1 complex was formed (Figure 7H).

DISCUSSION

The mechanisms of early mammalian cell fate determination remain to be elucidated due to the multiple layers of regulation.

A

Group	Blastocysts 3D (%)	Total cells (n)	Inner cells (%)	GFP cells (%)	Inner cells that are GFP+ (%)	GFP cells that are inner (%)
Gfp	65 (82.65)	41.91 ± 8.79	(37.68 ± 3.43)	(49.02 ± 3.44)	(53.06 ± 8.03) [x]	(40.51 ± 4.60) [x]
LincGET + i-*Carm1* + *Gfp*	62 (85.18)	41.85 ± 8.75	(36.20 ± 3.86)	(46.20 ± 5.75)	(43.06 ± 12.70) [y]	(32.89 ± 6.02) [y]

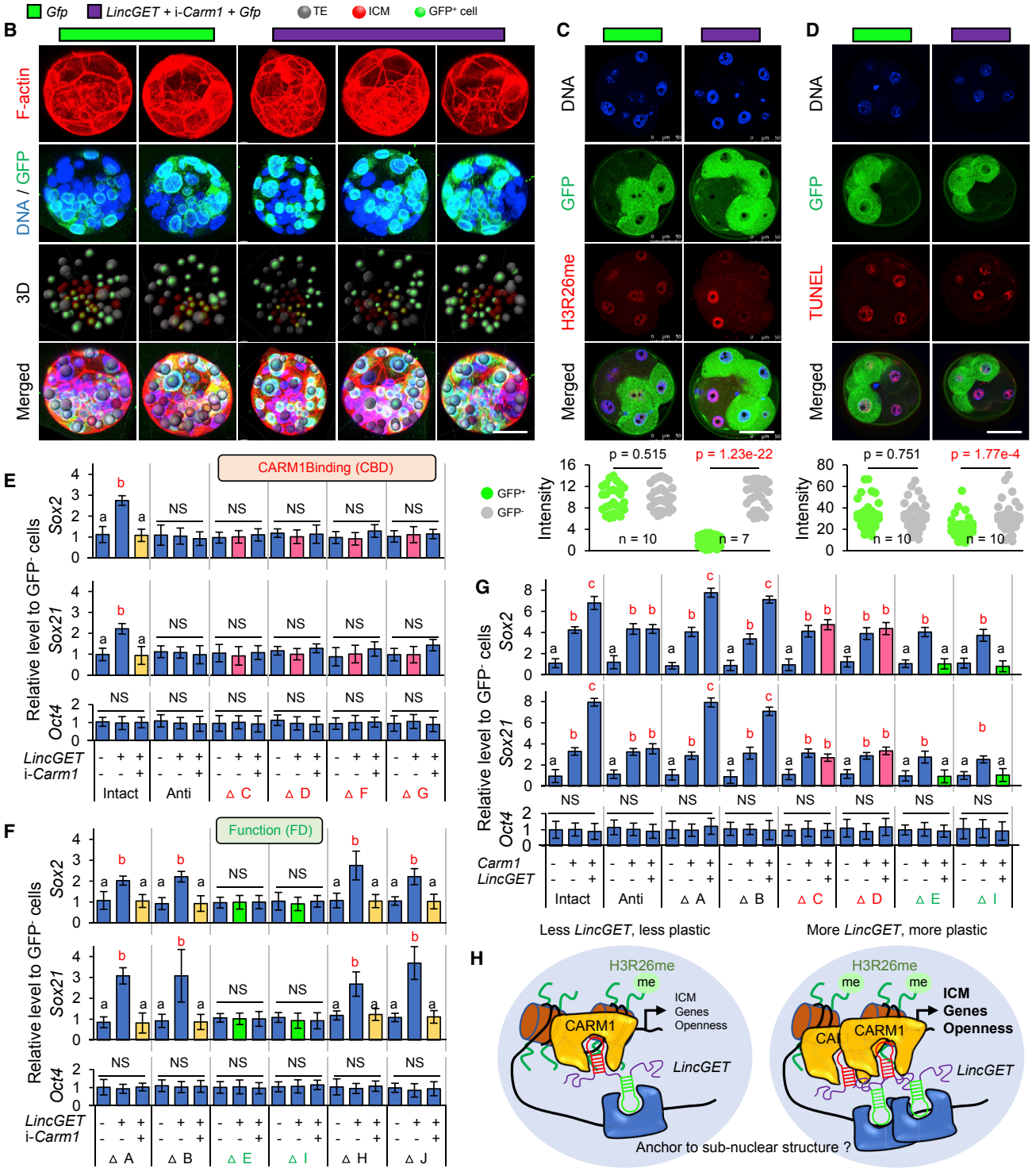

(legend on next page)

It remains debatable whether early blastomeres are equal in their developmental fate until the 16-cell stage or whether certain developmental bias already exists before the eight-cell stage, which predisposes early blastomeres toward either an ICM or a TE fate (Wennekamp et al., 2013; Zernicka-Goetz et al., 2009). Recent research advances have documented the molecular differences between early mammalian blastomeres as early as the four-cell stage. Epigenetic/genetic regulators such as CARM1/PRDM14, H3R26 methylation, DNA-binding dynamics of SOX2 or OCT4, and the level of SOX21 have shown heterogeneity between four-cell blastomeres to bias cell fate (Goolam et al., 2016; Piotrowska-Nitsche et al., 2005; Plachta et al., 2011; Tabansky et al., 2013; Torres-Padilla et al., 2007; White et al., 2016). However, the origin of the molecular heterogeneity observed at the four-cell stage remains an unresolved issue. Our data provide further evidence that the heterogeneous expression of *LincGET* at the late two-cell stage could act as an upstream regulator to influence subsequent lineage fate.

In fact, although two-cell blastomeres are generally considered to be totipotent, there are previous pieces of evidence and recent emerging reports showing that when two-cell blastomeres are separated, in the majority of cases, only one of the two-cell blastomeres develops into a mouse (Casser et al., 2017; Katayama et al., 2010; Morris et al., 2012; Papaioannou and Ebert, 1995; Tsunoda and McLaren, 1983). These data demonstrate inequality in the totipotency of two-cell blastomeres. Thus, our data regarding the heterogeneity of *LincGET* and its function in biasing lineage fate provide a molecular explanation for those experimental observations. The expression level of *LincGET* at the early two-cell embryo stage is almost absent, but it increases robustly at the late two-cell stage and shows heterogeneous expression between two-cell blastomeres (Figures 1 and S1). This suggests that the observed heterogeneity at the late two-cell embryo stage is generated *de novo* and thus may represent the gene expression noise that inevitably rises during ZGA, as previously reported (Shi et al., 2015). Alternatively, the heterogeneity of *LincGET* at the late two-cell stage may be triggered by unequally distributed unknown factors that already existed in the early two-cell embryos.

Early cleavage embryos are known to harbor many active ERVs, yet little is known about their functions (Evsikov et al., 2004; Peaston et al., 2004). It has been reported that MERVL transcription is a unique marker of two-cell mouse embryos and two-cell-like mESCs, which have higher pluripotency than that of normal mESCs (Macfarlan et al., 2012). In addition, embryonic chromatin at the two-cell stage has high core-histone mobility, and embryonic chromatin becomes progressively more compacted, losing plasticity and decreased developmental potency from totipotency to pluripotency (Bošković et al., 2014; Jachowicz et al., 2017). Active ERVs at the cleavage stage may have key roles in establishing totipotency to prepare materials for both TE and ICM lineage determination. There are numerous copies of ERV in the genome, which may provide an advantage for global chromatin opening. *LincGET* is a GLN-, MERVL-, and ERVK-associated lincRNA, and we found that increased *LincGET* expression enables ICM-specific gene promoters to become more open (Figure 6A). The origin of *LincGET* remains unknown, yet it raises the possibility that there might be other lncRNAs that are heavily associated with transposable elements that play important roles in early embryo development. In addition, we further propose that differential ERV activation resulting from ZGA may generate asymmetric patterns between two blastomeres, similar to *LincGET*, and thus may provide an additional resource for biasing embryonic fate.

As a recently identified lncRNA, we previously revealed the role of *LincGET* in controlling alternative splicing (Wang et al.,

Figure 7. Interdependence of *LincGET* and CARM1 in Directing ICM Fate

(A) The distribution of progeny of injected blastomere at the blastocyst stage based on 3D reconstruction analysis. Two-tailed Student's t tests were used for statistical analysis. Different letters between x and y indicate very significant differences ($p < 0.00001$). Key to table headings: blastocyst 3D (%) is the number and developmental rate of blastocysts that were all used for 3D analysis, total cells is the total number of cells in the blastocyst, inner cells (%) is the percentage of inner cells out of the total number of cells in the blastocyst, GFP cells (%) is the percentage of GFP-positive cells out of the total number of cells in the blastocyst, GFP cells that are inner (%) is the percentage of GFP-positive inner cells out of the total number of GFP-positive cells in the blastocyst, and inner cells that are GFP^+ (%) is the percentage of GFP-positive inner cells out of the total number of inner cells in the blastocyst.

(B) Examples of 3D analysis results. Scale bar, 50 μm.

(C) H3R26me2 staining shows that interference with *Carm1* could reduce H3R26me2 levels even in the presence of *LincGET* overexpression. Three experimental replicates were performed. For fluorescence analysis, the green ball stands for GFP^+ cells, and the gray ball stands for GFP^- cells. Two-tailed Student's t tests were used for statistical analysis. Scale bar, 50 μm.

(D) TUNEL fluorescent assay shows significantly lower levels of TUNEL fluorescence in daughter cells of *LincGET*-overexpressing and *Carm1*-depleted blastomeres. Three experimental replicates were performed. For fluorescence analysis, the green ball stands for GFP^+ cells, and the gray ball stands for GFP^- cells. Two-tailed Student's t tests were used for statistical analysis. Scale bar, 50 μm.

(E) qPCR results show that the truncated *LincGET* without CARM1 binding sites (Δ1,301–2,570 [ΔC–D] or Δ3,351–4,530 [ΔF–G]) failed to upregulate *Sox2* and *Sox21* in progeny blastomeres (red), and the intact *LincGET* exhibited no transcriptional activation activity when *Carm1* was depleted (orange). Three experimental replicates were performed. The error bars represent SEM. Two-tailed Student's t tests were used for statistical analysis. Different letters (a or b) indicate $p < 0.05$ (NS), $p > 0.05$.

(F) qPCR results show that some truncated *LincGET* mutants exhibited no transcriptional activation activity when *Carm1* was depleted (orange), and several truncated *LincGET* mutants (Δ 2,761–3,350 [ΔE] or Δ 5,121–5,710 [ΔI]) could bind to CARM1 but failed to upregulate *Sox2* and *Sox21* (green). Three experimental replicates were performed. The error bars represent SEM. Two-tailed Student's t tests were used for statistical analysis. Different letters (a or b) indicate $p < 0.05$ (NS), $p > 0.05$.

(G) qPCR results show that upregulation of *Sox2* and *Sox21* upon CARM1 overexpression could be cancelled by truncated *LincGET* (Δ 2,761–3,350 [ΔE] or Δ 5,121–5,710 [ΔI]). Three experimental replicates were performed. The error bars represent SEM. Two-tailed Student's t tests were used for the statistical analysis. Different letters (a, b, or c) indicate $p < 0.05$ (NS), $p > 0.05$.

(H) ICM bias model of the *LincGET*-CARM1 complex.

See also Figure S7 and Table S2.

2016). In addition to this mechanism, here, we further found that *LincGET* could upregulate *Sox2* and *Sox21* by forming a complex with CARM1, mostly in the nucleus. This supported the idea that in addition to the expression level, the intracellular location of the RNA/protein is essential in exerting proper functions. LncRNAs have emerged as key components of intracellular scaffolds that allow proper assembly of protein complexes, genes, and chromosomes subject to proper activation and deactivation (Batista and Chang, 2013). Intriguingly, another well-characterized lncRNA, *Neat1*, is also associated with transposable elements and is essential for the formation of a specific nuclear body structure called paraspeckle (Clemson et al., 2009; Lin et al., 2018). *LincGET* may function in a similar fashion to *Neat1* in terms of forming a scaffold and an "address code" for recruiting diffusible CARM1 and other essential proteins in the nucleus. Truncated *LincGET* (Δ2,761–3,350 [ΔE] or Δ 5,121–5,710 [ΔI]) could bind to CARM1 but failed to activate CARM1 target gene expression, and this may be due to the disruption of the scaffold region of *LincGET* that is essential for anchoring the complex to the correct intranuclear "address."

STAR★METHODS

Detailed methods are provided in the online version of this paper and include the following:

- KEY RESOURCES TABLE
- CONTACT FOR REAGENT AND RESOURCE SHARING
- EXPERIMENTAL MODEL AND SUBJECT DETAILS
  - Mouse embryos collection
  - Culture Cells
- METHOD DETAILS
  - RT-qPCR and 1C-qPCR
  - Plasmid vectors construction
  - CARM1 fractionation
  - Micro-injection
  - RNA pull-down
  - Western blotting
  - Mass spectrometry
  - Immunoprecipitation
  - Northern blotting
  - Immunofluorescence staining
  - RNA-FISH and IF combining RNA-FISH
  - Microscopic analysis and three-dimensional reconstructions
  - In vivo DNase I TUNEL assay
  - ATAC-seq library preparation and bioinformatic analyses of expression and heterogeneity in early embryo
- QUANTIFICATION AND STATISTICAL ANALYSIS
- DATA AND SOFTWARE AVAILABILITY
  - Data Resources

SUPPLEMENTAL INFORMATION

Supplemental Information includes seven figures and five tables and can be found with this article online at https://doi.org/10.1016/j.cell.2018.11.039.

ACKNOWLEDGMENTS

We thank Shiwen Li and Xili Zhu from the Institute of Zoology, Chinese Academy of Sciences, and Bofeng Liu, Wei Xie, and Yingying Gao from Tsinghua University for their technical assistance. This work was supported by grants from the Strategic Priority Research Program of the Chinese Academy of Sciences (XDA16030400 to Q.Z. and W.L.), National Natural Science Foundation of China (31621004 to Q.Z. and W.L., 31471395 to Q.Z.), the Key Research Projects of the Frontier Science of the Chinese Academy of Sciences (QYZDY-SSW-SMC002 to Q.Z.), the Key Deployment Projects of the Chinese Academy of Sciences (QYZDB-SSW-SMC022 to W.L.), the China Postdoctoral Science Foundation (2017M610990 and 2017T100107 to J.W.), the China National Postdoctoral Program for Innovative Talents (BX201700243 to L.W.), and the National Key Research and Development Program (2017YFA0103803 to Q.Z.).

AUTHOR CONTRIBUTIONS

J.W., W.L., and Q.Z. conceived and designed the study. J.W., L.W., G.F., Y.W., Y.L., X.L., C.L., G.J., and C.H. performed the experiments. J.W., L.W., G.F., J.S., T.Z., Q.C., Z.L., W.L., and Q.Z. analyzed the data. W.L. and Q.Z. supervised the project. J.W., G.F., Q.C., W.L., and Q.Z. designed and wrote the manuscript.

DECLARATION OF INTERESTS

The authors declare no competing interests.

Received: March 22, 2018
Revised: July 1, 2018
Accepted: November 22, 2018
Published: December 13, 2018

REFERENCES

Batista, P.J., and Chang, H.Y. (2013). Long noncoding RNAs: cellular address codes in development and disease. Cell *152*, 1298–1307.

Bošković, A., Eid, A., Pontabry, J., Ishiuchi, T., Spiegelhalter, C., Raghu Ram, E.V., Meshorer, E., and Torres-Padilla, M.E. (2014). Higher chromatin mobility supports totipotency and precedes pluripotency in vivo. Genes Dev. *28*, 1042–1047.

Burton, A., Muller, J., Tu, S., Padilla-Longoria, P., Guccione, E., and Torres-Padilla, M.E. (2013). Single-cell profiling of epigenetic modifiers identifies PRDM14 as an inducer of cell fate in the mammalian embryo. Cell Rep. *5*, 687–701.

Casser, E., Israel, S., Witten, A., Schulte, K., Schlatt, S., Nordhoff, V., and Boiani, M. (2017). Totipotency segregates between the sister blastomeres of two-cell stage mouse embryos. Sci. Rep. *7*, 8299.

Clemson, C.M., Hutchinson, J.N., Sara, S.A., Ensminger, A.W., Fox, A.H., Chess, A., and Lawrence, J.B. (2009). An architectural role for a nuclear noncoding RNA: NEAT1 RNA is essential for the structure of paraspeckles. Mol. Cell *33*, 717–726.

Deng, Q., Ramskold, D., Reinius, B., and Sandberg, R. (2014). Single-cell RNA-seq reveals dynamic, random monoallelic gene expression in mammalian cells. Science *343*, 193–196.

Evsikov, A.V., de Vries, W.N., Peaston, A.E., Radford, E.E., Fancher, K.S., Chen, F.H., Blake, J.A., Bult, C.J., Latham, K.E., Solter, D., and Knowles, B.B. (2004). Systems biology of the 2-cell mouse embryo. Cytogenet. Genome Res. *105*, 240–250.

Goolam, M., Scialdone, A., Graham, S.J.L., Macaulay, I.C., Jedrusik, A., Hupalowska, A., Voet, T., Marioni, J.C., and Zernicka-Goetz, M. (2016). Heterogeneity in Oct4 and Sox2 Targets Biases Cell Fate in 4-Cell Mouse Embryos. Cell *165*, 61–74.

Guttman, M., Donaghey, J., Carey, B.W., Garber, M., Grenier, J.K., Munson, G., Young, G., Lucas, A.B., Ach, R., Bruhn, L., et al. (2011). lincRNAs act in the circuitry controlling pluripotency and differentiation. Nature *477*, 295–300.

Hamazaki, N., Uesaka, M., Nakashima, K., Agata, K., and Imamura, T. (2015). Gene activation-associated long noncoding RNAs function in mouse preimplantation development. Development *142*, 910–920.

Hu, W., Alvarez-Dominguez, J.R., and Lodish, H.F. (2012). Regulation of mammalian cell differentiation by long non-coding RNAs. EMBO Rep. *13*, 971–983.

Jachowicz, J.W., Bing, X., Pontabry, J., Bošković, A., Rando, O.J., and Torres-Padilla, M.E. (2017). LINE-1 activation after fertilization regulates global chromatin accessibility in the early mouse embryo. Nat. Genet. *49*, 1502–1510.

Katayama, M., Ellersieck, M.R., and Roberts, R.M. (2010). Development of monozygotic twin mouse embryos from the time of blastomere separation at the two-cell stage to blastocyst. Biol. Reprod. *82*, 1237–1247.

Langmead, B., and Salzberg, S.L. (2012). Fast gapped-read alignment with Bowtie 2. Nat. Methods *9*, 357–359.

Lin, Y., Schmidt, B.F., Bruchez, M.P., and McManus, C.J. (2018). Structural analyses of NEAT1 lncRNAs suggest long-range RNA interactions that may contribute to paraspeckle architecture. Nucleic Acids Res. *46*, 3742–3752.

Liu, W., Liu, X., Wang, C., Gao, Y., Gao, R., Kou, X., Zhao, Y., Li, J., Wu, Y., Xiu, W., et al. (2016). Identification of key factors conquering developmental arrest of somatic cell cloned embryos by combining embryo biopsy and single-cell sequencing. Cell Discov. *2*, 16010.

Macfarlan, T.S., Gifford, W.D., Driscoll, S., Lettieri, K., Rowe, H.M., Bonanomi, D., Firth, A., Singer, O., Trono, D., and Pfaff, S.L. (2012). Embryonic stem cell potency fluctuates with endogenous retrovirus activity. Nature *487*, 57–63.

Morris, S.A., Guo, Y., and Zernicka-Goetz, M. (2012). Developmental plasticity is bound by pluripotency and the Fgf and Wnt signaling pathways. Cell Rep. *2*, 756–765.

Namekawa, S.H., and Lee, J.T. (2011). Detection of nascent RNA, single-copy DNA and protein localization by immunoFISH in mouse germ cells and preimplantation embryos. Nat. Protoc. *6*, 270–284.

Ng, S.Y., and Stanton, L.W. (2013). Long non-coding RNAs in stem cell pluripotency. Wiley Interdiscip. Rev. RNA *4*, 121–128.

Papaioannou, V.E., and Ebert, K.M. (1995). Mouse half embryos: viability and allocation of cells in the blastocyst. Dev. Dyn. *203*, 393–398.

Peabody, D.S. (1993). The RNA binding site of bacteriophage MS2 coat protein. EMBO J. *12*, 595–600.

Peaston, A.E., Evsikov, A.V., Graber, J.H., de Vries, W.N., Holbrook, A.E., Solter, D., and Knowles, B.B. (2004). Retrotransposons regulate host genes in mouse oocytes and preimplantation embryos. Dev. Cell *7*, 597–606.

Piotrowska-Nitsche, K., Perea-Gomez, A., Haraguchi, S., and Zernicka-Goetz, M. (2005). Four-cell stage mouse blastomeres have different developmental properties. Development *132*, 479–490.

Plachta, N., Bollenbach, T., Pease, S., Fraser, S.E., and Pantazis, P. (2011). Oct4 kinetics predict cell lineage patterning in the early mammalian embryo. Nat. Cell Biol. *13*, 117–123.

Rinn, J.L., and Chang, H.Y. (2012). Genome regulation by long noncoding RNAs. Annu. Rev. Biochem. *81*, 145–166.

Rossant, J., and Tam, P.P. (2009). Blastocyst lineage formation, early embryonic asymmetries and axis patterning in the mouse. Development *136*, 701–713.

Shi, J., Chen, Q., Li, X., Zheng, X., Zhang, Y., Qiao, J., Tang, F., Tao, Y., Zhou, Q., and Duan, E. (2015). Dynamic transcriptional symmetry-breaking in pre-implantation mammalian embryo development revealed by single-cell RNA-seq. Development *142*, 3468–3477.

Shin, H., Liu, T., Manrai, A.K., and Liu, X.S. (2009). CEAS: cis-regulatory element annotation system. Bioinformatics *25*, 2605–2606.

Shuai, L., Wang, Y., Dong, M., Wang, X., Sang, L., Wang, M., Wan, H., Luo, G., Gu, T., Yuan, Y., et al. (2015). Durable pluripotency and haploidy in epiblast stem cells derived from haploid embryonic stem cells in vitro. J. Mol. Cell Biol. *7*, 326–337.

Tabansky, I., Lenarcic, A., Draft, R.W., Loulier, K., Keskin, D.B., Rosains, J., Rivera-Feliciano, J., Lichtman, J.W., Livet, J., Stern, J.N., et al. (2013). Developmental bias in cleavage-stage mouse blastomeres. Curr. Biol. *23*, 21–31.

Torres-Padilla, M.E., Parfitt, D.E., Kouzarides, T., and Zernicka-Goetz, M. (2007). Histone arginine methylation regulates pluripotency in the early mouse embryo. Nature *445*, 214–218.

Tsunoda, Y., and McLaren, A. (1983). Effect of various procedures on the viability of mouse embryos containing half the normal number of blastomeres. J. Reprod. Fertil. *69*, 315–322.

Wang, J., Li, X., Wang, L., Li, J., Zhao, Y., Bou, G., Li, Y., Jiao, G., Shen, X., Wei, R., et al. (2016). A novel long intergenic noncoding RNA indispensable for the cleavage of mouse two-cell embryos. EMBO Rep. *17*, 1452–1470.

Wennekamp, S., Mesecke, S., Nédélec, F., and Hiiragi, T. (2013). A self-organization framework for symmetry breaking in the mammalian embryo. Nat. Rev. Mol. Cell Biol. *14*, 452–459.

White, M.D., Angiolini, J.F., Alvarez, Y.D., Kaur, G., Zhao, Z.W., Mocskos, E., Bruno, L., Bissiere, S., Levi, V., and Plachta, N. (2016). Long-Lived Binding of Sox2 to DNA Predicts Cell Fate in the Four-Cell Mouse Embryo. Cell *165*, 75–87.

Wu, J., Huang, B., Chen, H., Yin, Q., Liu, Y., Xiang, Y., Zhang, B., Liu, B., Wang, Q., Xia, W., et al. (2016). The landscape of accessible chromatin in mammalian preimplantation embryos. Nature *534*, 652–657.

Zernicka-Goetz, M., Morris, S.A., and Bruce, A.W. (2009). Making a firm decision: multifaceted regulation of cell fate in the early mouse embryo. Nat. Rev. Genet. *10*, 467–477.

Zhang, Y., Liu, T., Meyer, C.A., Eeckhoute, J., Johnson, D.S., Bernstein, B.E., Nusbaum, C., Myers, R.M., Brown, M., Li, W., and Liu, X.S. (2008). Model-based analysis of ChIP-Seq (MACS). Genome Biol. *9*, R137.